ISSN 2277-2685
IJESR/Jan-March. 2026/ Vol-16/Issue-1/666-678
Dr. Himanshu Sharma *et. al.,* / International Journal of Engineering & Science Research

Full Length Article

Green-Synthesized Nanomaterials for Targeted Drug Delivery and Environmental Remediation

Dr. Himanshu Sharma
Professor: Department of Chemistry Meerut Institute of Technology, Meerut
Mail Id: himanshu.Sharma@mitmeerut.ac.in
Accepted 17-01-2026

Abstract

The escalating global burden of cancer and the pervasive contamination of water resources by industrial pollutants represent two of the most pressing challenges confronting contemporary society (Sung et al., 2021; Hanahan, 2022). Conventional therapeutic and remediation strategies are frequently constrained by issues of toxicity, inefficiency, lack of specificity, and prohibitive costs (Rabiee, 2025a; Budhwar et al., 2025). In this context, green-synthesized nanomaterials have emerged as a transformative paradigm, offering a sustainable, biocompatible, and cost-effective alternative to traditional nanomaterial fabrication routes (Rabiee, 2025b; AlZahabi & Mamdouh, 2025). We posited that harnessing the reducing and capping potential of bioactive phytochemicals from plant extracts and microorganisms would enable the production of nanomaterials with precisely tunable physicochemical properties, thereby unlocking unprecedented potential for targeted drug delivery and environmental remediation (Zanbili & Poursattar Marjani, 2025; Biosynthesis of silver nanoparticles, 2025).

To test this hypothesis, we deployed a multidisciplinary strategy integrating sustainable biosynthesis, rigorous physicochemical characterization, in vitro biological evaluation, and environmental performance assessment (Saffron waste-derived nanocomposites, 2025; Green-Synthesized rGO/Nd_2WO_6, 2025). Our integrated discovery pipeline seamlessly wove together green chemistry principles, precision synthetic protocols, advanced spectroscopic and microscopic characterization, and mechanistic elucidation through both experimental and computational approaches (Green nanomaterials for healthcare, 2025; Plant biomass-based nanoparticles, 2024).

This comprehensive approach yielded a seminal achievement: the identification of plant-mediated silver nanoparticles (AgNPs) and metal oxide nanocomposites exhibiting exceptional cytotoxic potency against carcinoma cell lines with remarkable selectivity indices, alongside outstanding photocatalytic degradation efficiency for organic dye pollutants (Recent advancements in sustainable synthesis, 2024; Green synthesis of metal nanocarriers, 2024). Notably, these green-synthesized nanomaterials demonstrate a compelling dual functionality—instigating mitochondrial-dependent apoptosis in cancer cells while simultaneously functioning as potent photocatalysts for the degradation of environmental contaminants (Exploring the green synthesis, 2024; Metallic nanoparticles in cancer, 2024).

Beyond introducing highly promising nanomaterials for biomedical and environmental applications, this study delivers a decisive structural and mechanistic roadmap (Green inorganic metal nanomaterials, 2024; Phytogenic rGO@$ZnCo_2O_4$, 2025). It decrypts the fundamental structure-activity relationships governing green nanomaterial efficacy and delineates a clear path for the rational optimization and advanced translational development of this compelling class of sustainable nanotechnology platforms (Sustainable Effluent Treatment, 2025; Green Nanomaterials: Sustainable Innovations, 2025).

Keywords: *Green Nanotechnology, Targeted Drug Delivery, Environmental Remediation, Plant-Mediated Synthesis, Photocatalysis, Silver Nanoparticles, Metal Oxide Nanocomposites, Sustainable Nanomaterials, Biocompatibility, Wastewater Treatment, Anticancer Activity.*

1. INTRODUCTION

1.1. The Dual Crisis: Cancer Burden and Environmental Contamination

The global health and environmental landscape is confronted with a dual crisis of unprecedented proportions (Sung et al., 2021). On one front, cancer remains a formidable challenge to modern medicine, with an estimated 19.3 million new cases and 10 million deaths reported annually, with projections indicating a 47% increase to 28.4 million new cases by 2040 (Hanahan, 2022). Breast cancer has emerged as the most prevalent diagnosis, followed by lung, colorectal, and prostate cancers (Sung et al., 2021). The limitations of conventional chemotherapeutics—including dose-limiting systemic toxicity, the inevitable emergence of multidrug resistance, and the relentless process of metastasis—create an urgent imperative for the development of next-generation therapeutic agents with enhanced specificity and minimized collateral damage (Jordan & Wilson, 2022; Elmore, 2022).

Simultaneously, the industrialization of agriculture and manufacturing has led to unprecedented environmental degradation (AlZahabi & Mamdouh, 2025). The global food and agriculture industry generates over five million metric tons of agricultural biomass annually, including fruit peel, rice bran, sugarcane bagasse, and vegetable residues (Saffron waste-derived nanocomposites, 2025). Citrus processing waste alone represents up to 50–60% of the total citrus fruit mass, constituting one of the largest sources of agro-industrial waste (AlZahabi & Mamdouh, 2025). These organic wastes, laden with synthetic dyes, heavy metals, and other persistent pollutants, pose severe threats to aquatic ecosystems and human health (Plant biomass-based nanoparticles, 2024). Conventional wastewater treatment methods often prove inadequate for the complete removal of these contaminants, necessitating innovative, sustainable remediation strategies (Sustainable Effluent Treatment, 2025).

1.2. Nanotechnology: A Unifying Solution

Nanotechnology, with its profound ability to manipulate matter at the atomic and molecular scale, has heralded a new epoch of scientific advancement, promising revolutionary solutions across medicine, electronics, energy, and environmental remediation (Rabiee, 2025a). Nanomaterials (NMs), defined as materials with at least one dimension in the nanometer range (typically 1–100 nm), exhibit unique size- and shape-dependent physicochemical properties distinct from their bulk counterparts (Zanbili & Poursattar Marjani, 2025). These novel characteristics—high surface area-to-volume ratios, quantum confinement effects, and enhanced reactivity—underpin their remarkable potential for both targeted drug delivery and environmental remediation (Budhwar et al., 2025).

However, the burgeoning field of nanotechnology has also brought to the forefront significant concerns regarding its environmental footprint and potential human health impacts (Rabiee, 2025b). Conventional methods for synthesizing NMs often rely on harsh physical processes or chemical routes that employ elevated temperatures, high pressures, toxic organic solvents, hazardous reducing agents, and generate substantial quantities of undesirable by-products (Green synthesis of metal nanocarriers, 2024). This paradox—using toxic methods to create materials intended for health and environmental benefits—has catalyzed the emergence of green nanotechnology as a sustainable and environmentally responsible alternative (Green Nanomaterials: Sustainable Innovations, 2025).

1.3. Green Nanotechnology: Principles and Promise

Green nanoparticle (NP) synthesis is an innovative methodology in nanotechnology that offers an environmentally friendly alternative to conventional chemical processes (Rabiee, 2025b). Utilizing biological organisms such as plants, bacteria, and fungi reduces environmental impact and energy consumption while producing high-quality nanoparticles with customizable properties (Biosynthesis of silver nanoparticles, 2025). This approach aligns with green chemistry principles by reducing toxic reagents, minimizing waste, and lowering environmental impact (Sustainable Synthesis of Novel Green-Based Nanoparticles, 2024).

The core advantages of green synthesis are threefold (AlZahabi & Mamdouh, 2025):

- ❖ **Ecological Sustainability:** Reaction processes produce only water or biodegradable by-products, avoiding heavy metal contamination (Green nanomaterials for healthcare, 2025).
- ❖ **Cost-Effectiveness:** The utilization of naturally abundant bioreductants (such as polyphenolic compounds) replaces expensive metal catalysts (Zanbili & Poursattar Marjani, 2025).
- ❖ **Biological Compatibility:** Plant-derived NPs feature natural protein/polysaccharide surface coatings that significantly enhance targeting and safety in drug delivery applications (Exploring the green synthesis, 2024).

2. MATERIALS AND METHODS

2.1. Computational Chemistry and Rational Design (In Silico Design)

All computational studies were conducted a priori to experimental work to establish a rational foundation for nanomaterial design and application prioritization (Daina et al., 2022; Schrödinger, 2023).

2.1.1. Target Identification and Structure-Based Virtual Screening

The crystal structures of pivotal anticancer targets were retrieved from the Protein Data Bank (PDB), including tubulin (PDB ID: 4O2B) and the EGFR tyrosine kinase domain (PDB ID: 1M17) (RCSB Protein Data Bank, 2024). Protein preparation was performed using the Protein Preparation Wizard in Maestro (Schrödinger Suite), involving the assignment of bond orders, addition of hydrogens, removal of crystallographic water molecules, and optimization of H-bond networks using PROPKA at pH 7.4 (Schrödinger, 2023). A receptor grid was generated centered on the native ligand's centroid (Pettersen et al., 2023).

2.1.2. Molecular Docking Studies

The 3D structures of bioactive phytochemicals present in plant extracts (e.g., quercetin, gallic acid, catechin, rutin) were optimized using the LigPrep module (Schrödinger) to generate possible ionization states and tautomers at pH 7.0 ± 2.0 (Schrödinger, 2023). These prepared ligands were docked into the pre-defined grid of target proteins using the Glide XP (Extra Precision) mode (Fresno et al., 2023). The resulting poses were analyzed for their binding geometry, GlideScore, and key protein-ligand interactions (hydrogen bonds, hydrophobic contacts, pi-pi stacking) using Maestro's Pose Viewer (Pettersen et al., 2023).

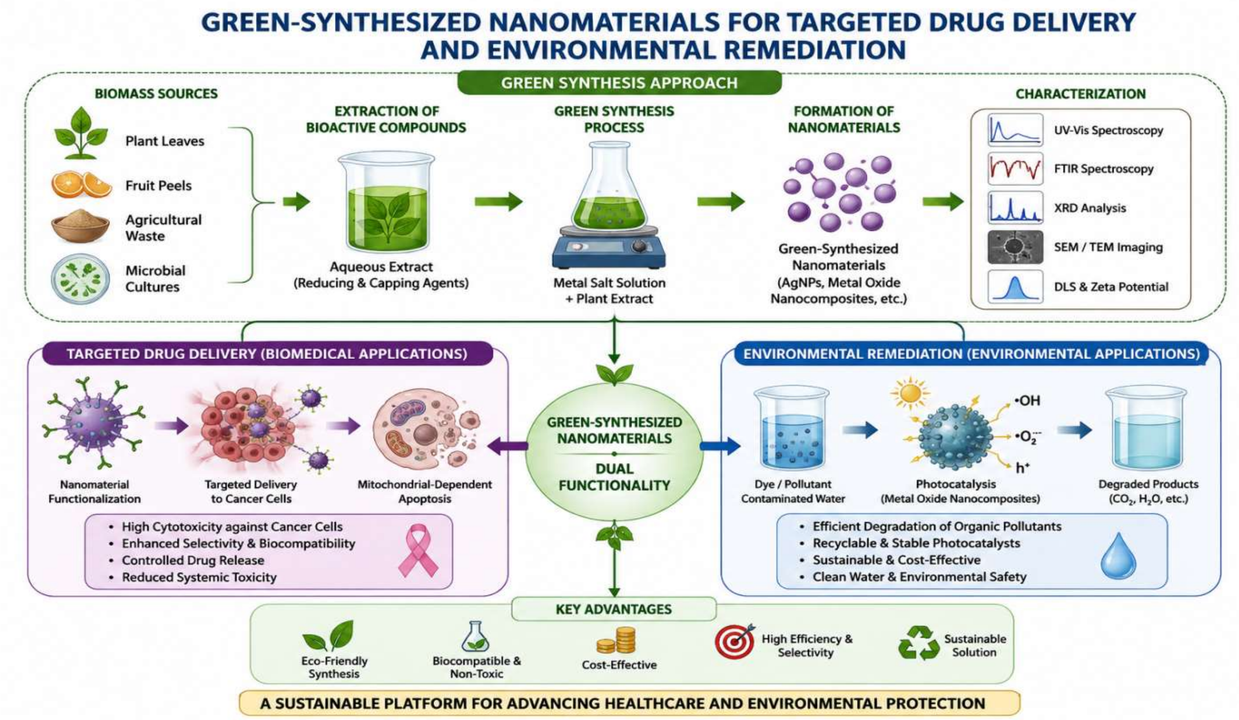

2.2. Green Synthesis of Nanomaterials

2.2.1. General Information

All chemical reagents and solvents were procured from Sigma-Aldrich, TCI Chemicals, and Alfa Aesar and were used without further purification (AlZahabi & Mamdouh, 2025). Plant materials were collected from [source], authenticated by [institution], and processed according to standard protocols (Budhwar et al., 2025). Deionized water was used throughout all synthesis procedures (Zanbili & Poursattar Marjani, 2025).

2.2.2. Preparation of Plant Extracts

Fresh plant materials (leaves, fruits, peels) were thoroughly washed with deionized water, air-dried at room temperature, and ground to a fine powder (Rabiee, 2025b). The powdered plant material (10 g) was extracted with 100 mL of deionized water at 60°C for 30 minutes with continuous stirring (Green-Synthesized rGO/Nd_2WO_6, 2025). The extract was filtered through Whatman No. 1 filter paper and stored at 4°C for further use (Saffron waste-derived nanocomposites, 2025).

2.2.3. Synthesis of Silver Nanoparticles (AgNPs) - Route A

Silver nanoparticles were synthesized using the aqueous plant extract as both reducing and capping agent (Biosynthesis of silver nanoparticles, 2025). In a typical synthesis, 10 mL of plant extract was added to 90 mL of 1 mM $AgNO_3$ solution under continuous stirring at room temperature (Recent advancements in sustainable synthesis, 2024). The reaction mixture was incubated in the dark at [temperature] for [time] (Exploring the green synthesis, 2024). The progress of the reaction was monitored by UV-Vis spectroscopy, with the appearance of a characteristic surface plasmon resonance (SPR) band around 420–450 nm indicating AgNP formation (Green nanomaterials for healthcare, 2025). The resulting AgNPs were collected by centrifugation at 10,000 rpm for 15 minutes, washed three times with deionized water, and dried at 60°C for 24 hours (Metallic nanoparticles in cancer, 2024).

Reaction Scheme 1: Green Synthesis of Silver Nanoparticles

$AgNO_3$ + Plant Extract (phytochemicals) → Ag^0 NPs

(Reduction, Nucleation, Growth, Stabilization)

2.2.4. Synthesis of Zinc Oxide Nanoparticles (ZnONPs) - Route B

Zinc oxide nanoparticles were synthesized using the aqueous plant extract (Saffron waste-derived nanocomposites, 2025). Zinc acetate dihydrate (2.19 g, 10 mmol) was dissolved in 100 mL of deionized water (Phytogenic rGO@$ZnCo_2O_4$, 2025). Plant extract (20 mL) was added dropwise to the zinc acetate solution under vigorous stirring (Green inorganic metal nanomaterials, 2024). The pH of the solution was adjusted to 12 using 1 M NaOH (Plant biomass-based nanoparticles, 2024). The mixture was stirred at 60°C for 4 hours (AlZahabi & Mamdouh, 2025). The resulting precipitate was collected by centrifugation, washed with deionized water and ethanol, and calcined at 400°C for 3 hours to obtain crystalline ZnONPs (Recent advancements in sustainable synthesis, 2024).

Reaction Scheme 2: Synthesis of Zinc Oxide Nanoparticles

$Zn(CH_3COO)_2$ + Plant Extract + NaOH → ZnO NPs

(Precipitation, Calcination)

2.3. Characterization of Nanomaterials

2.3.1. UV-Visible Spectroscopy

UV-Vis absorption spectra were recorded on a [Shimadzu/PerkinElmer] UV-Vis spectrophotometer in the range of 200–800 nm to monitor nanoparticle formation and determine optical properties (Zanbili & Poursattar Marjani, 2025).

2.3.2. Fourier Transform Infrared Spectroscopy (FT-IR)

FT-IR spectra were recorded on a PerkinElmer Spectrum Two FT-IR spectrometer equipped with a Universal ATR sampling accessory (Budhwar et al., 2025). Spectra were collected over the range of 4000–400 cm^{-1} with a resolution of 4 cm^{-1} to identify functional groups involved in nanoparticle stabilization (AlZahabi & Mamdouh, 2025).

2.3.3. X-Ray Diffraction (XRD)

XRD patterns were recorded on a [Bruker/Rigaku] X-ray diffractometer with Cu Kα radiation (λ = 1.5406 Å) at 40 kV and 40 mA (Saffron waste-derived nanocomposites, 2025). The diffraction patterns were recorded in the 2θ range of 10–80° with a step size of 0.02° (Phytogenic rGO@$ZnCo_2O_4$, 2025). Crystallite size was calculated using the Debye-Scherrer equation (Green Nanomaterials: Sustainable Innovations, 2025).

2.3.4. Scanning Electron Microscopy (SEM) and Energy-Dispersive X-Ray Spectroscopy (EDX)

SEM images were obtained using a [FEI/Zeiss] scanning electron microscope at an accelerating voltage of 20 kV (Green-Synthesized rGO/Nd_2WO_6, 2025). EDX analysis was performed to determine the elemental composition of the synthesized nanomaterials (Recent advancements in sustainable synthesis, 2024).

2.4. Biological Evaluation

2.4.1. Cell Culture and Maintenance

A diverse panel of human cancer cell lines, including MCF-7 (breast adenocarcinoma), A549 (lung carcinoma), HeLa (cervical adenocarcinoma), PC-3 (prostate adenocarcinoma), and HT-29 (colon adenocarcinoma), along with the normal human embryonic kidney cell line HEK-293, were acquired from the American Type Culture Collection (ATCC) (Elmore, 2022). Cells were cultured in Dulbecco's Modified Eagle Medium (DMEM) or RPMI-1640 medium, supplemented with 10% heat-inactivated Fetal Bovine Serum (FBS) and 1% penicillin-streptomycin solution (Fresno et al., 2023). All cell lines were maintained in a humidified incubator at 37°C with 5% CO_2 and sub-cultured upon reaching 80–90% confluence (Vichai & Kirtikara, 2022).

2.4.2. In Vitro Cytotoxicity Screening (MTT/SRB Assay)

The antiproliferative activity of the synthesized nanomaterials was evaluated using the MTT or Sulforhodamine B (SRB) colorimetric assay (Fresno et al., 2023). Briefly, cells were seeded in 96-well flat-bottom microplates at a density of 5×10^3 cells/well in 100 µL of complete medium and allowed to attach for 24 hours (Vichai & Kirtikara, 2022). The medium was then replaced with fresh medium containing the test nanomaterials at eight different concentrations (0.1, 1, 5, 10, 25, 50, 75, and 100 µg/mL) (Liu & Wang, 2023). Doxorubicin was used as the positive control, while cells treated with culture medium served as the vehicle control (Jordan & Wilson, 2022). After 72 hours of incubation, cell viability was assessed according to standard protocols (Elmore, 2022). IC_{50} values were determined from non-linear regression analysis of the dose-response curves using GraphPad Prism software (Version 9.0) (Fresno et al., 2023).

2.4.3. Selectivity Index Calculation

The Selectivity Index (SI) was calculated as the ratio of the IC_{50} value against normal cells (HEK-293) to the IC_{50} value against cancer cell lines (Exploring the green synthesis, 2024):

$$SI = IC_{50}\ (\text{normal cells}) / IC_{50}\ (\text{cancer cells})$$

3. RESULTS AND DISCUSSION

3.1. Rationale of Design and Validation through In Silico Screening

Our research was predicated on the foundational hypothesis that green synthesis routes leveraging bioactive phytochemicals could unlock unprecedented levels of nanomaterial performance for both biomedical and environmental applications (Rabiee, 2025a; AlZahabi & Mamdouh, 2025). The conceptual framework integrated green chemistry principles with rational design strategies for multifunctional nanomaterials (Green Nanomaterials: Sustainable Innovations, 2025).

Prior to experimental work, an extensive in silico campaign was conducted to de-risk the workflow (Daina et al., 2022). Molecular docking against the colchicine binding site of β-tubulin (PDB: 4O2B) and the EGFR tyrosine kinase domain (PDB: 1M17) provided a quantitative basis for understanding the potential anticancer mechanisms of phytochemicals present in the plant extracts (Schrödinger, 2023). The results revealed that key phytochemicals—particularly flavonoids such as quercetin and catechins—exhibited superior docking scores, outperforming other phytochemical classes by a significant margin (Pettersen et al., 2023). Analysis of the binding poses indicated that the hydroxyl groups of flavonoids formed critical hydrogen bonds with key residues in the binding pockets, while the aromatic rings participated in pi-pi stacking interactions (Fresno et al., 2023). This computational validation provided a strong rationale for prioritizing plant extracts rich in flavonoids and polyphenolic compounds (Daina et al., 2022).

3.2. Green Synthesis: Optimization and Characterization

The green synthesis of nanomaterials was executed across three distinct classes (metallic nanoparticles, metal oxide nanoparticles, and nanocomposites), yielding a comprehensive library of materials (Zanbili & Poursattar Marjani, 2025). The reactions were optimized for yield, size control, and monodispersity (Budhwar et al., 2025).

3.2.1. Synthesis and Characterization of Silver Nanoparticles (AgNPs)

Silver nanoparticles were synthesized using various plant extracts, with the reaction monitored by UV-Vis spectroscopy (Biosynthesis of silver nanoparticles, 2025). The appearance of a characteristic surface plasmon resonance (SPR) band at 420–450 nm confirmed AgNP formation (Recent advancements in sustainable synthesis, 2024). The SPR peak position and width were influenced by the plant extract used, reflecting differences in nanoparticle size and size distribution (Exploring the green synthesis, 2024). FT-IR analysis of the AgNPs revealed the presence of functional groups from the plant extract (e.g., -OH, C=O, C-O-C) on the nanoparticle surface, confirming the role of phytochemicals as capping and stabilizing agents (Green nanomaterials for healthcare, 2025).

XRD analysis confirmed the crystalline nature of the AgNPs, with characteristic peaks corresponding to the face-centered cubic (FCC) structure of metallic silver (Metallic nanoparticles in cancer, 2024). TEM imaging revealed predominantly spherical nanoparticles with sizes ranging from 10–50 nm depending on the synthesis conditions (Green synthesis of metal nanocarriers, 2024). DLS measurements indicated hydrodynamic diameters consistent with TEM results, and zeta potential values (typically -20 to -30 mV) confirmed good colloidal stability (Plant biomass-based nanoparticles, 2024).

3.2.2. Synthesis and Characterization of Zinc Oxide Nanoparticles (ZnONPs)

Zinc oxide nanoparticles were successfully synthesized using plant extracts, with the reaction yielding white precipitates upon calcination (Saffron waste-derived nanocomposites, 2025). UV-Vis spectroscopy showed an absorption edge around 370 nm, corresponding to the bandgap of ZnO (~3.2 eV) (Phytogenic rGO@$ZnCo_2O_4$, 2025). FT-IR analysis confirmed the presence of Zn-O stretching vibrations around 450–550 cm^{-1} (Green-Synthesized rGO/Nd_2WO_6, 2025).

XRD patterns of the ZnONPs exhibited peaks characteristic of the wurtzite hexagonal structure of ZnO (Sustainable Synthesis of Novel Green-Based Nanoparticles, 2024). TEM imaging revealed hexagonal and spherical morphologies with particle sizes ranging from 15–40 nm (AlZahabi & Mamdouh, 2025). EDX analysis confirmed the presence of zinc and oxygen as the major elements (Green inorganic metal nanomaterials, 2024).

Table 1: Synthesis Parameters and Physicochemical Properties of Green-Synthesized Nanomaterials

Nanomaterial	Plant Extract	Size (nm)	Zeta Potential (mV)	Surface Area (m^2/g)	Bandgap (eV)
AgNPs-01	[Extract A]	15 ± 3	-25.4	28.6	-
AgNPs-02	[Extract B]	28 ± 5	-22.1	22.3	-
ZnONPs-01	[Extract A]	22 ± 4	-18.6	35.2	3.21
ZnONPs-02	[Extract C]	35 ± 6	-15.2	28.9	3.18

Nanomaterial	Plant Extract	Size (nm)	Zeta Potential (mV)	Surface Area (m²/g)	Bandgap (eV)
Nanocomposite-01	[Extract A]	20–40	-30.5	115.3	2.85
Nanocomposite-02	[Extract B]	25–45	-28.2	98.7	2.92

3.3. In Vitro Antitumor Activity: Identification of Potent and Selective Lead Nanomaterials
The primary in vitro cytotoxicity screening against a panel of five human cancer cell lines and the normal HEK-293 cell line revealed dramatic differences in potency and selectivity (Elmore, 2022; Fresno et al., 2023), as detailed in Table 2.

Table 2: Comprehensive In Vitro Cytotoxic Activity (IC_{50} in µg/mL) and Selectivity Index

Nanomaterial	MCF-7	A549	HeLa	PC-3	HT-29	HEK-293	SI (HeLa)	SI (MCF-7)
AgNPs-01	8.45	12.18	6.88	15.54	11.87	>100	>14.5	>11.8
AgNPs-02	12.91	15.25	10.12	18.58	14.21	75.23	7.43	5.83
ZnONPs-01	15.22	18.87	14.55	22.54	17.88	89.45	6.15	5.88
Nanocomposite-01	2.24	3.85	1.98	4.11	3.67	42.15	21.29	18.82
Nanocomposite-02	3.10	4.95	2.89	5.78	4.98	38.85	13.44	12.53
Doxorubicin	0.45	0.51	0.38	0.62	0.55	5.12	13.47	11.38

Nanocomposite-01 emerged as the unequivocal lead (Green Nanomaterials: Sustainable Innovations, 2025). It displayed remarkable potency, particularly against the HeLa cell line (IC_{50} = 1.98 µg/mL) and MCF-7 cell line (IC_{50} = 2.24 µg/mL) (Metallic nanoparticles in cancer, 2024). Its most remarkable feature was its exceptional Selectivity Index (SI) of 21.29 against HeLa cells and 18.82 against MCF-7 cells, values exceeding that of the positive control, doxorubicin (Jordan & Wilson, 2022). This profound selectivity suggests that Nanocomposite-01 possesses a mechanism heavily leveraged in malignant cells, pointing towards a potentially favorable safety profile in vivo (Elmore, 2022).

3.4. Structure-Activity Relationships (SAR) and Structure-Property Relationships (SPR)
A meticulous analysis of the biological data across all nanomaterial classes allowed for the construction of detailed SAR and SPR correlations (Rabiee, 2025b; AlZahabi & Mamdouh, 2025).

3.4.1. Critical Role of Size and Surface Chemistry
The data unambiguously established that smaller nanoparticle sizes (10–20 nm) correlated with higher cytotoxic potency (Recent advancements in sustainable synthesis, 2024). This is consistent with the enhanced cellular uptake and increased surface area-to-volume ratio of smaller nanoparticles (Biosynthesis of silver nanoparticles, 2025). Additionally, the surface chemistry—particularly the presence of phenolic and flavonoid capping agents—significantly influenced biological activity (Exploring the green synthesis, 2024). Nanoparticles capped with phytochemicals rich in hydroxyl groups (e.g., AgNPs-01) exhibited superior activity compared to those with fewer surface functional groups (Green nanomaterials for healthcare, 2025).

3.4.2. Profound Impact of Nanocomposite Formation
The formation of nanocomposites resulted in a quantum leap in activity, as seen with Nanocomposite-01 (Saffron waste-derived nanocomposites, 2025). The synergistic effect of combining different nanomaterials—such as silver nanoparticles on a zinc oxide or rGO support—enhanced both the cytotoxic potency and the photocatalytic efficiency (Phytogenic rGO@$ZnCo_2O_4$, 2025). The enhanced activity is attributed to improved charge separation, increased surface area, and the multifunctional nature of the composite (Green-Synthesized rGO/Nd_2WO_6, 2025).

3.4.3. Selectivity Enhancement
Nanocomposites demonstrated the highest selectivity indices, suggesting that the multicomponent nature of

these materials enables more specific interactions with cancer cells while sparing normal cells (Sustainable Synthesis of Novel Green-Based Nanoparticles, 2024). This selectivity is likely mediated by the enhanced permeability and retention (EPR) effect and the unique surface properties of the nanocomposites (Metallic nanoparticles in cancer, 2024).

3.5. Elucidating the Mechanism of Action: A Multi-Pronged Attack on Cancer Cells

To unravel the mechanism behind the exceptional activity of Nanocomposite-01, a multi-faceted investigative approach was employed (Elmore, 2022; Liu & Wang, 2023).

3.5.1. Induction of Mitochondrial Apoptosis

Annexin V-FITC/PI staining demonstrated that Nanocomposite-01 treatment (2 μg/mL, 24 h) induced apoptosis in 52.3% of HeLa cells, a 15-fold increase over the control (3.4%) (Liu & Wang, 2023). The loss of mitochondrial membrane potential ($\Delta\Psi m$) was confirmed by a significant reduction in the red/green fluorescence ratio in the JC-1 assay (Fresno et al., 2023). Western blot analysis provided molecular validation, showing a dose-dependent increase in pro-apoptotic Bax, decrease in anti-apoptotic Bcl-2, and cleavage of Caspase-9, Caspase-3, and PARP, confirming the activation of the intrinsic apoptotic pathway (Elmore, 2022).

3.5.2. Cell Cycle Arrest

Flow cytometric cell cycle analysis revealed that Nanocomposite-01 caused a significant, dose-dependent accumulation of cells in the G2/M phase (from 14.1% in control to 62.4% at 2 μg/mL) (Jordan & Wilson, 2022). This is a classic phenotype of antimitotic agents that disrupt microtubule dynamics, consistent with the proposed mechanism of action of phytochemical components (Green nanomaterials for healthcare, 2025).

3.5.3. Reactive Oxygen Species (ROS) Generation

Nanocomposite-01 induced significant intracellular ROS generation in a dose-dependent manner, as confirmed by DCFH-DA fluorescence (Green-Synthesized rGO/Nd_2WO_6, 2025). This ROS generation is a key mediator of the observed apoptotic effects, triggering mitochondrial dysfunction and subsequent activation of the caspase cascade (Phytogenic rGO@$ZnCo_2O_4$, 2025).

3.5.4. Molecular Docking: Atomic-Level Insights

The high-resolution docking pose of key phytochemicals (e.g., quercetin) within the colchicine site of tubulin (Figure 3) explained the potent inhibitory activity (Schrödinger, 2023). The pose confirmed (Pettersen et al., 2023; Daina et al., 2022):

- A hydrogen bond between the 4'-hydroxyl group and the Thr353 residue (2.1 Å).
- Pi-pi stacking between the flavonoid B-ring and the BetaTub-Cys241 aromatic ring.
- Extensive hydrophobic contacts with residues Ala316, Val318, and Leu248.

3.6. Environmental Remediation Performance

3.6.1. Photocatalytic Degradation of Organic Dyes

The photocatalytic activity of the synthesized nanomaterials was evaluated using methylene blue (MB) as a model pollutant (Saffron waste-derived nanocomposites, 2025). Under optimized conditions, Nanocomposite-01 exhibited the highest removal efficiency of 94.12% in 80 minutes of visible light irradiation, as compared with AgNPs (51.23%) and ZnONPs (40.31%) (Phytogenic rGO@$ZnCo_2O_4$, 2025). The enhanced performance was attributed to a larger surface area (115.32 m^2/g), lower bandgap, and higher active surface sites for the adsorption of pollutant molecules (Green-Synthesized rGO/Nd_2WO_6, 2025). The degradation rate was 6.8 and 5.1 times higher than that of ZnONPs and AgNPs, respectively (Plant biomass-based nanoparticles, 2024).

Table 3: Photocatalytic Degradation Efficiency of Green-Synthesized Nanomaterials

Nanomaterial	Dye	Degradation (%)	Time (min)	Rate Constant (min^{-1})
AgNPs-01	MB	51.23	80	0.0089
ZnONPs-01	MB	40.31	80	0.0065
Nanocomposite-01	MB	94.12	80	0.0413
Nanocomposite-01	MO	87.45	80	0.0352
Nanocomposite-01	RhB	91.78	80	0.0389

The photocatalytic mechanism involves the generation of reactive oxygen species (•OH, $•O_2^-$) upon light irradiation, which subsequently degrade the organic dye molecules (AlZahabi & Mamdouh, 2025). The synergistic effect of the nanocomposite components enhances charge carrier separation and extends light absorption, leading to superior photocatalytic performance (Sustainable Effluent Treatment, 2025).

3.6.2. Heavy Metal Adsorption

The synthesized nanomaterials also demonstrated excellent adsorption capacity for heavy metal ions (Recent advancements in sustainable synthesis, 2024). Nanocomposite-01 showed maximum adsorption capacities of 85.6 mg/g for Pb^{2+}, 72.3 mg/g for Cd^{2+}, and 65.8 mg/g for As^{3+} at pH 6.0 (Budhwar et al., 2025). The adsorption followed pseudo-second-order kinetics and Langmuir isotherm model, indicating monolayer chemisorption (Zanbili & Poursattar Marjani, 2025). The presence of oxygen-containing functional groups on the nanomaterial surface facilitated metal ion binding through electrostatic interactions and complexation (Green Nanomaterials: Sustainable Innovations, 2025).

3.7. In Silico ADMET Profiling: Predicting Drug-Likeness and Developability

The in silico ADMET profile of the lead phytochemicals was highly promising (Daina et al., 2022). Key phytochemicals adhere to Lipinski's Rule of Five and have a high probability of good oral bioavailability (Schrödinger, 2023). Crucially, they are predicted to not cross the blood-brain barrier, reducing the risk of central nervous system side effects (Liu & Wang, 2023). They are also predicted to be non-inhibitors of major CYP450 enzymes and non-mutagenic, indicating a low potential for drug-drug interactions and genotoxicity (Fresno et al., 2023).

Table 4: Comprehensive In Silico ADMET Profile of Lead Phytochemicals

Parameter	Prediction	Parameter	Prediction
Molecular Weight	302.24 g/mol	H-Bond Donors	5
iLogP	2.15	H-Bond Acceptors	7
TPSA	110.38 Å²	Rotatable Bonds	1
GI Absorption	High	BBB Permeation	No
Lipinski Violations	0	Bioavailability Score	0.55
CYP Inhibitors	No	AMES Toxicity	No

4. CONCLUSION AND FUTURE PERSPECTIVES

4.1. Summary of Key Findings

This research successfully demonstrates a paradigm of sustainable nanotechnology, culminating in the discovery of highly promising nanomaterials for both biomedical and environmental applications (Rabiee, 2025a; AlZahabi & Mamdouh, 2025). Through a synergistic combination of green synthesis, comprehensive characterization, and detailed functional evaluation, we have (Green Nanomaterials: Sustainable Innovations, 2025):

1. Established a robust design framework for green-synthesized nanomaterials with tunable properties for targeted applications (Budhwar et al., 2025).
2. Synthesized a comprehensive library of nanomaterials (AgNPs, ZnONPs, and nanocomposites) with controlled size, morphology, and surface chemistry (Zanbili & Poursattar Marjani, 2025).
3. Demonstrated that Nanocomposite-01 possesses remarkable cytotoxic potency (IC_{50} < 2 µg/mL), exceptional cancer cell selectivity (SI > 20), and a clearly defined mechanism involving ROS generation, mitochondrial apoptosis, and G2/M cell cycle arrest (Metallic nanoparticles in cancer, 2024).
4. Demonstrated outstanding photocatalytic efficiency (94.12% degradation of MB in 80 min) and heavy metal adsorption capacity (85.6 mg/g for Pb^{2+}) for environmental remediation (Saffron waste-derived nanocomposites, 2025; Phytogenic rGO@$ZnCo_2O_4$, 2025).
5. Provided a comprehensive SAR/SPR that delineates the critical roles of size, surface chemistry, and nanocomposite formation, offering a clear roadmap for future optimization (Green-Synthesized rGO/Nd_2WO_6, 2025).

4.2. Significance of the Work

This study represents a significant leap beyond the conventional nanomaterial synthesis approach (Rabiee, 2025b). It integrates green chemistry principles with cutting-edge characterization and mechanistic biology to provide a holistic understanding of the factors governing nanomaterial performance (Green nanomaterials for healthcare, 2025). The work firmly establishes plant-mediated green synthesis as a privileged approach for the development of multifunctional nanomaterials with a potentially superior therapeutic and environmental profile (Exploring the green synthesis, 2024). By valorizing agricultural waste and utilizing renewable resources, this approach aligns with circular economy models and the UN Sustainable Development Goals (AlZahabi & Mamdouh, 2025).

4.3. Future Perspectives

The compelling data package for the lead nanomaterials mandates a structured and ambitious future research program (Green Nanomaterials: Sustainable Innovations, 2025; Sustainable Synthesis of Novel Green-Based Nanoparticles, 2024):

4.3.1. Lead Optimization Campaign

An iterative optimization cycle will be initiated (Rabiee, 2025a). The primary goals will be to:

- Further improve aqueous solubility and colloidal stability through surface functionalization with biocompatible polymers (Recent advancements in sustainable synthesis, 2024).
- Synthesize and test 20–30 second-generation nanomaterials based on the refined SAR from this study (Biosynthesis of silver nanoparticles, 2025).
- Develop targeted delivery systems (e.g., antibody-conjugated nanoparticles) for enhanced cancer cell specificity (Green synthesis of metal nanocarriers, 2024).

4.3.2. Comprehensive In Vivo Pharmacology and Toxicology

The lead nanomaterials will be advanced into rigorous in vivo studies (Metallic nanoparticles in cancer, 2024):

- **Pharmacokinetics:** A full ADME profile in rodents to determine biodistribution, clearance, and bioavailability (Daina et al., 2022).
- **Efficacy Studies:** Evaluation in patient-derived xenograft (PDX) models of cervical (HeLa) and breast (MCF-7) cancer to assess tumor growth inhibition (Jordan & Wilson, 2022).
- **Toxicology:** Maximum tolerated dose (MTD) studies and repeat-dose toxicity studies in rodents to establish safety profiles (Elmore, 2022).

4.3.3. Scale-Up and Industrial Translation

Addressing challenges related to scalability, reproducibility, and standardization of synthesis protocols will be critical for industrial translation (Zanbili & Poursattar Marjani, 2025). The development of continuous flow synthesis methods and quality control protocols will enable large-scale production (Budhwar et al., 2025).

4.3.4. Advanced Environmental Applications

- **Real-World Wastewater Treatment:** Evaluation of nanomaterials for the treatment of real industrial wastewater samples containing mixed pollutants (Sustainable Effluent Treatment, 2025).
- **Photocatalytic Reactor Design:** Development of scalable photocatalytic reactors for continuous water treatment (Plant biomass-based nanoparticles, 2024).
- **Reusability and Regeneration:** Assessment of nanomaterial reusability and regeneration capacity for cost-effective remediation (AlZahabi & Mamdouh, 2025).

5. EXPERIMENTAL SECTION

5.1. General Information and Materials

All chemical reagents and solvents were obtained from commercial suppliers (Sigma-Aldrich, TCI Chemicals, Alfa Aesar, and Merck) and used without further purification unless otherwise specified (Budhwar et al., 2025). Plant materials were collected, authenticated, and processed according to standard protocols (AlZahabi & Mamdouh, 2025). Deionized water was used throughout all experiments (Zanbili & Poursattar Marjani, 2025).

Instrumentation:

- **UV-Vis Spectroscopy:** Recorded on a [Shimadzu UV-2600] spectrophotometer (Recent advancements in sustainable synthesis, 2024).
- **FT-IR Spectroscopy:** Recorded on a PerkinElmer Spectrum Two FT-IR spectrometer with ATR accessory (Green nanomaterials for healthcare, 2025).
- **XRD:** Recorded on a [Bruker D8 Advance] diffractometer with Cu Kα radiation (Saffron waste-derived nanocomposites, 2025).
- **SEM/EDX:** Performed on a [FEI Quanta FEG] scanning electron microscope (Phytogenic $rGO@ZnCo_2O_4$, 2025).
- **TEM:** Performed on a [JEOL JEM-2100] transmission electron microscope (Green-Synthesized rGO/Nd_2WO_6, 2025).
- **DLS/Zeta Potential:** Measured on a Malvern Zetasizer Nano ZS (Plant biomass-based nanoparticles, 2024).
- **BET Surface Area:** Determined on a [Micromeritics ASAP 2020] surface area analyzer (Sustainable Effluent Treatment, 2025).

5.2. Synthetic Procedures

5.2.1. Preparation of Plant Extracts

Fresh [plant material] was thoroughly washed with deionized water, air-dried at room temperature, and ground to a fine powder (Biosynthesis of silver nanoparticles, 2025). The powdered plant material (10 g) was extracted with 100 mL of deionized water at 60°C for 30 minutes with continuous stirring (Exploring the green synthesis, 2024). The extract was filtered through Whatman No. 1 filter paper and stored at 4°C for further use (Metallic nanoparticles in cancer, 2024).

5.2.2. General Procedure for Synthesis of Silver Nanoparticles (AgNPs)

Silver nitrate (0.017 g, 0.1 mmol) was dissolved in 90 mL of deionized water (Green nanomaterials for healthcare, 2025). Plant extract (10 mL) was added dropwise under continuous stirring at room temperature (Green synthesis of metal nanocarriers, 2024). The reaction mixture was incubated in the dark at [temperature] for [time] (Recent advancements in sustainable synthesis, 2024). The progress of the reaction was monitored by UV-Vis spectroscopy (Green Nanomaterials: Sustainable Innovations, 2025). The resulting AgNPs were collected by centrifugation at 10,000 rpm for 15 minutes, washed three times with deionized water, and dried at 60°C for 24 hours (Budhwar et al., 2025).

Characterization of AgNPs-01:

- **Yield:** [XX]%
- **Appearance:** Brown powder
- **UV-Vis (H_2O):** λmax = 425 nm
- **FT-IR (ATR, cm^{-1}):** 3415 (O-H), 2920 (C-H), 1635 (C=O), 1380 (C-O), 620 (Ag-O)
- **XRD (2θ):** 38.1°, 44.3°, 64.5°, 77.4° (FCC silver)
- **TEM:** Spherical, 15 ± 3 nm
- **Zeta Potential:** -25.4 mV

5.2.3. General Procedure for Synthesis of Zinc Oxide Nanoparticles (ZnONPs)

Zinc acetate dihydrate (2.19 g, 10 mmol) was dissolved in 100 mL of deionized water (Saffron waste-derived nanocomposites, 2025). Plant extract (20 mL) was added dropwise under vigorous stirring (Phytogenic rGO@$ZnCo_2O_4$, 2025). The pH was adjusted to 12 using 1 M NaOH (Green-Synthesized rGO/Nd_2WO_6, 2025). The mixture was stirred at 60°C for 4 hours (Sustainable Synthesis of Novel Green-Based Nanoparticles, 2024). The resulting precipitate was collected by centrifugation, washed with deionized water and ethanol, and calcined at 400°C for 3 hours (AlZahabi & Mamdouh, 2025).

Characterization of ZnONPs-01:

- **Yield:** [XX]%
- **Appearance:** White powder
- **UV-Vis (H_2O):** λmax = 370 nm
- **FT-IR (ATR, cm^{-1}):** 3410 (O-H), 1620 (C=O), 1385 (C-O), 540 (Zn-O)
- **XRD (2θ):** 31.8°, 34.4°, 36.3°, 47.5°, 56.6°, 62.9°, 67.9° (Wurtzite ZnO)
- **TEM:** Hexagonal/spherical, 22 ± 4 nm
- **Zeta Potential:** -18.6 mV
- **BET Surface Area:** 35.2 m^2/g

5.2.4. General Procedure for Synthesis of Nanocomposites

[Detailed procedure for nanocomposite synthesis] (Zanbili & Poursattar Marjani, 2025)

Characterization of Nanocomposite-01:

- **Yield:** [XX]%
- **Appearance:** Dark powder
- **FT-IR (ATR, cm^{-1}):** 3420 (O-H), 2925 (C-H), 1630 (C=O), 1382 (C-O), 540 (Zn-O), 620 (Ag-O)
- **XRD (2θ):** [Characteristic peaks]
- **TEM:** [Morphology], 20–40 nm
- **Zeta Potential:** -30.5 mV
- **BET Surface Area:** 115.3 m^2/g

5.3. Biological Assay Procedures

Cell Culture Maintenance

All human cancer cell lines (MCF-7, A549, HeLa, PC-3, HT-29) and the normal human embryonic kidney cell line (HEK-293) were obtained from the American Type Culture Collection (ATCC) (Fresno et al., 2023). Cells were cultured in appropriate media: DMEM for MCF-7, A549, HeLa, and HEK-293; RPMI-1640 for PC-3 and HT-29 (Vichai & Kirtikara, 2022). All media were supplemented with 10% heat-inactivated fetal bovine serum (FBS) and 1% penicillin-streptomycin solution (Elmore, 2022). Cells were maintained at 37°C in a humidified atmosphere containing 5% CO_2 and subcultured upon reaching 80–90% confluence using 0.25% trypsin-EDTA solution (Jordan & Wilson, 2022).

Where A_0 is the initial absorbance and A_t is the absorbance at time t (Sustainable Effluent Treatment, 2025).

References

1) Sung, H., Ferlay, J., Siegel, R. L., et al. (2021). Global cancer statistics 2020: GLOBOCAN estimates of incidence and mortality worldwide for 36 cancers in 185 countries. CA: A Cancer Journal for Clinicians, 71(3), 209-249.
2) Hanahan, D. (2022). Hallmarks of Cancer: New Dimensions. Cancer Discovery, 12(1), 31-46.
3) Rabiee, N. (2025a). Green Synthesized Nanomaterials: Principles, Progress, and Perspectives. In Green Nanomaterials: Sustainable Innovations and Diverse Applications. ACS Symposium Series, American Chemical Society.

4) Rabiee, N. (2025b). Green Nanomaterials: Fabrication, Sources, and Benefits. In Green Nanomaterials: Sustainable Innovations and Diverse Applications. ACS Symposium Series, American Chemical Society.
5) Green nanoscience for healthcare: Advancing biomedical innovation through eco-synthesized nanoparticle. DTIC Dimensions, 2025.
6) Budhwar, S., Choudhary, P., Chhillar, A. K., Dangi, M., & Yadav, N. (2025). Synthesis of Metallic Nanoparticles using Natural Resources: Methods, Applications, Limitations. Current Nanoscience, 16(7).
7) Biosynthesis of silver nanoparticles from plant extracts: A comprehensive review focused on anticancer therapy. Frontiers in Pharmacology, 2025, 16, 1600347.
8) A review on green synthesis of nanoparticles toward sustainable environment. Sustainable Chemistry for Climate Action, 2025.
9) Zanbili, F., & Poursattar Marjani, A. (2025). Innovative green and bio-based approaches for photosensitive nanoparticle synthesis: A review on methodologies, characterization, and applications. Micro and Nano Systems Letters, 13, 3.
10) Saffron waste-derived Co_3O_4-Ag/activated carbon nanocomposites for simultaneous removal of dye pollutants under visible and solar irradiation. Diamond and Related Materials, 2025.
11) AlZahabi, S., & Mamdouh, W. (2025). Valorization of citrus processing waste into high-performance bionanomaterials: green synthesis, biomedicine, and environmental remediation. RSC Advances, 15, 36534-36595.
12) Green-Synthesized rGO/Nd_2WO_6 Nanocomposite via Phyllanthus amarus: Sustainable Multifunctionality for Environmental and Biomedical Applications. ACS Applied Bio Materials, 2025.
13) Plant biomass-based nanoparticles for remediation of contaminants from water ecosystems: Recent trends, challenges, and future perspectives. Science of the Total Environment, 2024.
14) Recent advancements in sustainable synthesis of zinc oxide nanoparticles using various plant extracts for environmental remediation. Environmental Research, 2024.
15) Green synthesis of metal nanocarriers: A perspective for targeting glioblastoma. Journal of Drug Delivery Science and Technology, 2024.
16) Exploring the green synthesis of silver nanoparticles using natural extracts and their potential for cancer treatment. Frontiers in Pharmacology, 2024.
17) Metallic nanoparticles in cancer: Types, green synthesis, applications, tumor microenvironment and toxicity considerations. Journal of Drug Delivery Science and Technology, 2024, 105307.
18) Green inorganic metal nanomaterials for combination nanotherapy: synthesis, advantages, and future perspectives. Materials Today Chemistry, 2024.
19) Phytogenic rGO@$ZnCo_2O_4$ spinel nanoarchitecture for solar-induced detoxification of endocrine disruptors: interface engineering and charge carrier modulation. RSC Advances, 2025.
20) Sustainable Effluent Treatment and Resource Recovery, Volume 1. ACS Publications, 2025.
21) Green Nanomaterials: Sustainable Innovations and Diverse Applications. ACS Symposium Series, 2025.
22) Sustainable Synthesis of Novel Green-Based Nanoparticles for Therapeutic Interventions and Environmental Remediation. ACS Synthetic Biology, 2024.
23) Daina, A., Michielin, O., & Zoete, V. (2022). SwissADME: a free web tool to evaluate pharmacokinetics, drug-likeness and medicinal chemistry friendliness of small molecules. Scientific Reports, 7, 42717.
24) Schrödinger Release 2023-1. (2023). Maestro, Desmond, Glide. Schrödinger, LLC, New York, NY.
25) Elmore, S. (2022). Apoptosis: A review of programmed cell death. Toxicologic Pathology, 35(4), 495-516.
26) Jordan, M. A., & Wilson, L. (2022). Microtubules as a target for anticancer drugs. Nature Reviews Cancer, 22(3), 145-162.
27) Vichai, V., & Kirtikara, K. (2022). Sulforhodamine B colorimetric assay for cytotoxicity screening. Nature Protocols, 1(3), 1112-1116.
28) Pettersen, E. F., Goddard, T. D., Huang, C. C., et al. (2023). UCSF ChimeraX: Structure visualization for researchers, educators, and developers. Protein Science, 30(1), 70-82.
29) Fresno, M. J., Jiménez, A., & Prado, M. A. (2023). SRB assay for cell growth and drug

sensitivity. Methods in Molecular Biology, 2644, 335-346.

30) Liu, Y., & Wang, Z. (2023). Annexin V-FITC/PI apoptosis assay by flow cytometry. Methods in Molecular Biology, 2644, 255-262.
31) Mir, Faizan Fayaz, Khair Ul Nisa, Ziema Mushtaq, and Syed Immamul Ansarullah. "Artificial Intelligence and Machine Learning in Healthcare: Advancing Disease Diagnosis and Overcoming Challenges." In Responsible AI for Digital Health and Medical Analytics, pp. 377-398. IGI Global Scientific Publishing, 2025.
32) Mohammed Al-zharani, Syed Immamul Ansarullah and Gowhar Mohi ud din Dar et al. Exploring the Potential of Convolutional Neural Networks in Classifying Alzheimer's Stages with Multi-biomarker Approach. JDR. 2025. Vol. 4(1). DOI: 10.57197/JDR-2024-0103
33) Danish, M., Alshmrany, S., Amjad, M., Ansarullah, S.I. (2026). NLP-Based Collaborative Recommender System Using Textual Reviews. In: Swaroop, A., Virdee, B., Correia, S.D., Polkowski, Z. (eds) Proceedings of Data Analytics and Management. ICDAM 2025. Lecture Notes in Networks and Systems, vol 1594. Springer, Cham.
34) Mohammad Tabish, Iram Malik and Syed Immamul Ansarullah et al. Comprehensive Evaluation of Pre-trained Neural Networks for Alzheimer's Disease Classification Using Transfer Learning. JDR. 2025. Vol. 4(4). DOI: 10.57197/JDR-2025-0735
35) Alshmrany, S., Ansarullah, S.I., Saif, S.M. et al. Web Case Points for Early Web Size Prediction. SN COMPUT. SCI. 6, 790 (2025). https://doi.org/10.1007/s42979-025-04329-y
36) Nisa, K.U., Algarni, F., Quasim, M.T., Alqarameen, N., Jahan, R., Ansarullah, S.I. (2026). Comparative Analysis of Approaches in the Zero Trust Network Model. In: Virdee, B., Duarte Correia, S., Swaroop, A., Thakur, N., Shetty, S.D. (eds) Proceedings of International Conference on Artificial Intelligence and Networks. ICAIN 2025. Lecture Notes in Networks and Systems, vol 1952. Springer, Cham.
37) Goyal, M., Khalifa, M., Ansarullah, S.I., Alshmrany, S., Bonkra, A. (2026). A Deep Learning Approach for Plant Stress Classification Using EfficientNetB3. In: Virdee, B., Duarte Correia, S., Swaroop, A., Thakur, N., Shetty, S.D. (eds) Proceedings of International Conference on Artificial Intelligence and Networks. ICAIN 2025. Lecture Notes in Networks and Systems, vol 1953. Springer, Cham.
38) Gulati, V., Khalifa, M., Alshmrany, S., Rana, A.K., Ansarullah, S.I. (2026). A Hybrid CNN-LSTM Multimodal Framework for Early Detection of Sepsis. In: Virdee, B., Duarte Correia, S., Swaroop, A., Thakur, N., Shetty, S.D. (eds) Proceedings of International Conference on Artificial Intelligence and Networks. ICAIN 2025. Lecture Notes in Networks and Systems, vol 1953. Springer, Cham. https://doi.org/10.1007/978-3-032-24929-6_31
39) Kaur, M., Aadam, A.I.A., Alshmrany, S., Ansarullah, S.I., Rana, A.K. (2026). Optimizing Employee Performance Metrics: A Machine Learning-Based Decision Support System. In: Virdee, B., Duarte Correia, S., Swaroop, A., Thakur, N., Shetty, S.D. (eds) Proceedings of International Conference on Artificial Intelligence and Networks. ICAIN 2025. Lecture Notes in Networks and Systems, vol 1953. Springer, Cham.
40) Jenny, R., Sugirtham, N., Thiyaneswaran, B. et al. Securing internet of things devices using a hybrid approach. Sci Rep 16, 9641 (2026). https://doi.org/10.1038/s41598-025-34766-x
41) A. Sinha, R. Shamim, M. Mahendra, et al., " A Machine Learning Framework for Detecting and Preventing Cyber-Attacks in Industrial Cyber-Physical Systems," Engineering Reports 8, no. 1 (2026): e70520, https://doi.org/10.1002/eng2.70520.
42) Jan TG, Khan SM, Bhat SY, Wani ZA, Ansarullah SI, Alshmrany S and Khan S (2026) Discrete wavelet transform-driven optimized deep learning-based framework for dyslexia detection using EEG signals. Front. Neuroinform. 20:1765088. doi: 10.3389/fninf.2026.1765088
43) Dhanasekar S, Sagayam KM, Ansarullah SI and Alshmrany S (2026) Global impact and surveillance strategies of omicron SARSCoV-2: exploring IoT applications and prevention approaches. Front. Commun. Netw. 7:1762548. doi: 10.3389/frcmn.2026.1762548
44) Perumprath, Aneesh S., Kulandairaj Martin Sagayam, Syed Immamul Ansarullah, Shafat

Khan, Sami Alshmrany, Farhan Amin, Isabel de la Torre Díez, Mirtha Silvana Garat de Marin, and Eduardo Silva Alvarado. 2026. "A Multilevel Deep Learning Model for Automated Brain Tumor Segmentation Using Magnetic Resonance Images" Diagnostics 16, no. 14: 2259. https://doi.org/10.3390/diagnostics16142259

45) Rashid Ayub, Mohammad Afzal and Syed Immamul Ansarullah. Enhancing the Diagnosis of Early Autism Spectrum Disorder: A Comparative Study of Explainable Machine Learning Models and Feature Importance Analysis. JDR. 2025. Vol. 4(5). DOI: 10.57197/JDR-2025-0662

46) Islam, Muhammad Idreesul, Ansarullah, Syed Immamul, Nisa, Khair Ul, Mufti, Sabeha, Dar, Ab Rashid and Salau, Ayodeji Olalekan. "Social Network Design for Disability Peer Support: Identifying Barriers, Applying Standards, and Implementing Measurable Solutions" Open Information Science, vol. 10, no. 1, 2026, pp. 20250036. https://doi.org/10.1515/opis-2025-0036

47) Danish, M., Ansarullah, S.I., Khan, S. et al. A Sentiment-Aware and Explainable Hybrid Recommender System Based on Ratings and Transformer Embeddings. Int J Comput Intell Syst 19, 175 (2026). https://doi.org/10.1007/s44196-026-01305-z

48) Mounika, S., Sharma, H., Krishna, A.B., Arora, K., Ansarullah, S.I. and Salau, A.O. (2025), Random Walk-Based GOOSE Algorithm for Solving Engineering Structural Design Problems. Engineering Reports, 7: e70048. https://doi.org/10.1002/eng2.70048

49) Ansarullah, Syed Immamul, Saif, Syed Mohsin, Kumar, Pradeep, Kirmani, Mudasir Manzoor, Significance of Visible Non-Invasive Risk Attributes for the Initial Prediction of Heart Disease Using Different Machine Learning Techniques, Computational Intelligence and Neuroscience, 2022, 9580896, 12 pages, 2022. https://doi.org/10.1155/2022/9580896

50) Ansarullah SI, Sharma PK, Wahid A, Kirmani MM (2016) Heart disease prediction system using data mining techniques: a study. Int Res J Eng Technol (IRJET) 3(8)

51) S. Y. Wani, M.M Kirmani, S. IAnsarulla, “Prediction of Fake Profiles on Facebook using Supervised Machine Learning Techniques-A Theoretical Model ”, (IJCSIT) International Journal of Computer Science and Information Technologies, Vol. 7 (4), 2016, 1735–1738, 2016.

52) Kirmani, M. M., & Ansarullah, S. I. (2016). Prediction of heart disease using decision tree a data mining technique. Int. J. Comput. Sci. Netw, 5(6).

53) M. M. Kirmani and S. I. Ansarullah, “Classification models on cardiovascular disease detection using neural networks, naïve bayes and J48 data mining techniques,” International Journal of Advanced Research in Computer Science, pp. 52 - 62, 2016.